JAERI-M
82-171

JAPANESE CONTRIBUTIONS TO IAEA INTOR WORKSHOP, PHASE II A

CHAPTER IV : PLASMA CONFINEMENT AND CONTROL

November 1982

Kenro MIYAMOTO*1, Masayoshi SUGIHARA
Kojyu UEDA*2, Shin YAMAMOTO, Masaki MAENO
Seio SENGOKU, Norio SUZUKI, Satoshi KASAI
Masayuki NAGAMI, Takashi TUDA, Keiji TANI
Masao OKAMOTO*3 and Noboru FUJISAWA

日 本 原 子 力 研 究 所
Japan Atomic Energy Research Institute

JAERI-M レポートは，日本原子力研究所が不定期に公刊している研究報告書です。
入手の問合わせは，日本原子力研究所技術情報部情報資料課（〒319－11 茨城県那珂郡東海村）あて，お申しこしください。なお，このほかに財団法人原子力弘済会資料センター（〒319-11 茨城県那珂郡東海村日本原子力研究所内）で複写による実費頒布をおこなっております。

JAERI-M reports are issued irregularly.
Inquiries about availability of the reports should be addressed to Information Section, Division of Technical Information, Japan Atomic Energy Research Institute, Tokai-mura, Naka-gun, Ibaraki-ken 319-11, Japan.

© Japan Atomic Energy Research Institute, 1982

編集兼発行　日本原子力研究所
印　　刷　山田軽印刷所

JAERI-M 82-171

Japanese Contributions to IAEA INTOR Workshop, Phase IIA

Chapter IV: Plasma Confinement and Control

Kenro MIYAMOTO[*1], Masayoshi SUGIHARA, Kojyu UEDA[*2],
Shin YAMAMOTO, Masaki MAENO, Seio SENGOKU,
Norio SUZUKI, Satoshi KASAI, Masayuki NAGAMI,
Takashi TUDA, Keiji TANI, Masao OKAMOTO[*3] and Noboru FUJISAWA

Fusion Research and Development Center
Tokai Research Establishment, JAERI

(Received October 30, 1982)

This report corresponds to Chapter IV of Japanese contribution report to IAEA INTOR workshop, Phase IIA. Studies are centered on confinement performance of INTOR core plasmas, losses induced by toroidal field ripples and discharge controls indispensable to long burn.

Keywords: INTOR, Confinement Time, High Beta, Ripple Loss, Burn Control, Position Control, Disruptions.

---

*1) The University of Tokyo

*2) Mitsubishi Electric Co., Ltd.

*3) Nagoya University

JAERI-M 82-171

INTORフェーズⅡAワークショップ検討報告書
第Ⅳ章：プラズマの閉込めと制御

日本原子力研究所東海研究所
核融合研究開発推進センター
宮本健郎[*1]・杉原正芳・上田孝寿[*2]・山本　新
前野勝樹・仙石盛夫・鈴木紀男・河西　敏
永見正幸・津田　孝・谷　啓二・岡本正雄[*3]
藤沢　登

（1982年10月30日受理）

このレポートは，IAEA INTOR フェーズⅡAワークショップへの国内の検討報告書の第Ⅳ章に相当するものである。イントール炉心プラズマの閉込め性能，トロイダル磁場リップルにより生じる損失，長時間運転に必要な放電の制御を検討したものである。

＊1）東京大学
＊2）三菱電機㈱
＊3）名古屋大学

Contents

目　　次

1. Plasma Confinement and β Limit

1.1. Experimental status

1.1.1. Neutral beam heating experiments in the JFT-2 tokamak

S. Yamamoto, M. Maeno, S. Sengoku, N. Suzuki, S. Kasai
and JFT-2 Group

§1. Introduction

High-beta plasmas are required for the tokamak approach to an economic fusion reactor. Therefore it is essential to obtain a high-β tokamak plasma and characteristics of the high-β plasma have to be investigated. Many experimental studies on high-β plasma have been started in tokamak devices [1,2,3,4]. To obtain high beta plasmas, a 2 MW neutral beam injection (NBI) system and a 1 MW ioncyclotron range of frequency (ICRF) system were installed on the JFT-2 tokamak. A top view of the device and the diagonostic is shown in Fig. IV-1-1. The NBI system consists of a co- and a counter-injector with the injection angle of 40° to the plasma axis. Each beam line has the maximum ion current of 65 A at 40 kV and the maximum power of each neutral beam measured at the injection port is 1 MW. An almost circular plasma investigated under a wide range of plasma parameters, i.e. $R/a = 3.5 - 4.75$, $q_a = 2.0 - 4.2$, $n_{e0} = (2.5 - 16) \times 10^{13}$ cm^{-3}, and $B_T = 0.95 - 1.4$ T, NBI heating of 0.8 - 2 MW, where R/a, q_a, n_{e0} and B_T are aspect ratio, safety factor, central plasma density and toroidal magnetic field, respectively. In this paper, properties of plasma confinement and impurity transport in JFT-2 plasmas subject to intense heating are described.

§2. Beta values [3,4]

Measured β-values are compared with the critical β-values obtained from the ballooning analysis. The critical β-value from the ballooning analysis is very sensitive to the pressure profile. An optimized pressure profile at the critical values [5] is compared with the experimental data. Figure IV-1-2 shows the measured central beta value β_0, and the volume-averaged beta value, $<\beta>$, versus the safety factor q_a. The beam powers lie in the range between 0.8 and 1.2 MW. Open points indicate the thermal contribution to beta, and solid points designate the thermal and fast-ion beam contributions. The striped bands show critical peaked beta values and volume-averaged beta values from high-n ballooning-mode analysis [5]. The lower lines of each band indicate the critical values for $q_o = 1$ and the upper lines those for $q_o = 0.9$, respectively. The total beta values including the beam component are higher than the calculated critical beta values, in many discharges. It must, however, be noted that the maximum thermal beta values are only slightly higher than the theoretical values.

Recently, a maximum volume averaged beta $<\beta>$ up to 3%, due to thermal components, has been achieved with 1 MW co- and 1 MW counter-injection at line integrated density $\bar{n}_e = 1.2 \times 10^{14}$ cm^{-3}, and plasma current I_p=140 kA [6]. The calculated poloidal beta β_p from the volume averaged beta is 2.6 due to the thermal components, but the β_p from magnetic measurements, i.e. poloidal field and vertical field measurement, is 1.8 - 2.3. If we consider uncertainties of the temperature and the density profile, especially the ion density, the calculated β_p from the density and temperature should be 2.0 - 2.7 due to the thermal components.

§3. Transport

In order to study the influence of high power heating on plasma confinement, we investigated the dependence of the poloidal beta values β_p on additional heating power. Both a magnetic measurement and a diamagneitc measurement are used. The increment of β_p with 1 MW counter-injection is 0.6 - 0.7 times as small as that with 1 MW co-injection. The large loss power in counter-injection is due to the relatively low plasma currents ($I_p = 130$ - 145 kA) in JFT-2 and is consistent with the Monte-Carlo calculation. In the case of the two beams, 1 MW counter-beam (which corresponds to 1.6 - 1.7 MW co-injection), the increment of β_p is additive. Figure IV-1-3 shows $\Delta(\Lambda + 1) \equiv \Delta(\beta_p + \ell_i/2)$ versus net input power P_{NET}, including the cases of NBI, ICRF and also simultaneous heating of NBI and ICRF, where ℓ_i is plasma internal inductance. Compared with ohmic heating, NBI heating makes, in general, the electron temperature profiles broader and thus reduces internal inductance ℓ_i. Typically, the calculated change in ℓ_i is much less than the change in β_p. Thus, the figure reflects mainly variation in β_p. The experimental results show that up to the power level of 2.2 MW (1.7 MW NBI and 0.5 MW ICRF), the increment of β_p is proportional to the net input power.

Figure IV-1-4(a) shows the global energy confinement time evaluated at r = a versus line integrated density $\bar{n}_e$. The global energy confinement time in the beam heated discharges appears to be a weak function of $\bar{n}_e$ compared with the ohmically heated plasma as shown in Fig. IV-1-4(b) Figure IV-1-5(a) shows the dependence of β_p versus I_p, at $\bar{n}_e = 5 \times 10^{13}$ cm^{-3} with 1 MW co-injection. The lower lines of each band indicate the values for $\ell_i = 1$ and the upper lines those for $\ell_i = 0.5$. The result shows that the values of $\beta_p \cdot I_p$ is nearly constant. Figure IV-1-5(b)

shows the dependence of $\Lambda + 1$ versus B_T at $\bar{n}_e = 5 \times 10^{13}$ cm^{-3} and $I_p = 80$ kA with 1 MW co-injection and 0.5 MW counter-injection. These experimental results suggest that global energy confinement time τ_E is significantly improved increasing plasma current, because $\tau_E \propto \beta_p I_p^2 = (\beta_p \cdot I_p) I_p \propto I_p$. While, the energy confinement time appears to be only weakly dependent on B_T.

Global particle confinement time τ_p is measured by the electrostatic double probe method. Global particle confinement time is defined as $\tau_p = N_e/F$, where F is the total loss flux to the first wall and the limiter. Figure IV-1-6 shows the particle confinement time versus $\sqrt{q_a}\,\bar{n}_e$. The relation $\tau_p \propto \sqrt{q}\,\bar{n}_e$ was confirmed in DIVA tokamak [7]. particle confinement time in beam heated discharge is reduced compared with ohmically heated plasma. But the maximum reduction of τ_p is 20 to 30 percent. Not appreciable difference was found between co-injection and counter-injection as for reduction of τ_p, although not many cases were taken with counter-injection.

The observed temperature and β-value are analyzed by using a tokamak code including, NBI heating, neutral particle transport and the sawtooth effect [4]. The sawtooth repetition time and the amplitude of the sawtooth oscillations in the NBI heating phase are greater than the corresponding values of classical sawtooth oscillations with ohmic heating. Figure IV-1-7 shows an example of simulations for beam induced (enhanced) sawtooth oscillations. The results suggest that the transport in the high-β plasma is about the same in a low-β plasma within a factor of 2, i.e. $\chi_e = 3 - 4 \times 10^{17}/n_e$ cm^2/s, $D \approx 0.3\,\chi_e$ and $\chi_i = 3 - 4\,\chi_{NC}$ where n_e is plasma density in cm^{-3} and χ_{NC} the neoclassical value.

§4. Density Clamp [8]

The density clamp was observed in both cases of co- and counter-injection. This phenomenon is due to deterioration of particle confinement and/or decreased recycling of neutrals from the wall or limiter. A simple particle balance equation is written as follows.

$$dN_e/dt = - N_e/\tau_p + R\, N_e/\tau_p + S$$

$$= -(1 - R)\, N_e/\tau_p + S$$

where τ_p: particle confinement time, R: recycling rate,

S: total gas influx including neturals from beam lines.

Figure IV-1-8 shows the results of the typical measurements. Neutral beam were injected at density ramping phase. Although hydrogen gas was continuously puffed in, density was clamped by the injection (Fig. IV-1-8(a)). The limiter flux and the wall flux increased with the injection. Boundary electron temperature determined by the limiter probe also increases (Fig. IV-1-8(b)). Particle confinement time τ_p in the beam heated discharge decreases about 25 % and the trapping efficiently (1-R) becomes almost doubled (Fig. IV-1-8(c)). These experimental results show that for the observed change of dN_e/dt, contribution of the enhanced trapping efficinecy is larger than the contribution of dcreased particle confinement time. Therefore enhancement of the trapping efficiency during the injection is the dominant cause of the density clamping. This density clamping is easily suppressed by intense gas puffing, and this does not set the upper limit of the plasma density.

§5. Plasma rotation [9]

Toroidal plasma rotation induced by the momentum input associated with unbalanced neutral beam injection was investigated in order to clarify the effect upon tokamak transport processes. Rotational velocities of the plasma were estimated from Doppler shifts of appropriate spectra lines (TiXIV, OVII and CV). Figure IV-1-9 shows the measured radial profile and time evolutions of radial profiles and time evolutions of toroidal plasma velocities in the relatively low density region ($\bar{n}_e = (3 - 4) \times 10^{13} cm^{-3}$). Before the neutral-beam pulse, a central velocity of $\sim 1.3 \times 10^6$ cm/s in the counter-direction is seen. The maximum rotational velocity near the centre is $V_\phi(\sim 5$ cm) $\sim 1.5 \times 10^6$ cm/s, corresponding to 1 MW co-injection, for hydrogen beam into hydrogen plasma ($H^o \rightarrow H^+$). On the other hand, relatively high density region ($\bar{n}_e = (6 - 7) \times 10^{13}$ cm^{-3}), rotational velocity is smaller than 1×10^6 cm/s, corresponding to 1 MW co-injection, for hydrogen beam into deuterium plasma ($H^o \rightarrow D^+$). In JFT-2, high-β plasma is obtained in relatively high density region with two simultaneous beams. In the relatively low density region, the central ion thermal velocity is several times as large as the plasma rotational velocity. The decrease in the central ion temperature with increasing density is less rapid than $1/\bar{n}_p$, for the above mentioned range of plasma densities [10]. These experimental results suggest that plasma rotation does not play an important role in transport processes of high beta plasma in high density region.

§6. Inpurity Transport [11]

To study the beam effects on the impurity transport, the radial line radiation profiles of iron which is intrinsic impurity from wall or limiter, were measured during the neutral beam injection. The plasma conditions are nearly the same in both cases of 1 MW co- and 1 MW counter-injection, exhibiting "sawtooth" behaviors. The radial profiles of iron line radiation in co- (solid lines) and counter-injection (dashed lines) shown in Fig. IV-1-10 are taken 30 ms after starting the NBI heating. Soft x-ray (PIN-Diode) signals along the central chord over the whole duration of the discharge are also shown in the figure. These signals show that rapid impurity accumulation does not take place during counter injection. On the other hand, in both cases of co- and counter-injection, the amount of metal impurities at the plasma centre increases corresponding to the increase of the impurity influx due to ion sputtering, if we do not control neutral gas influx, as shown in Fig. IV-1-11 [10]. These experimental results show that the neoclassical, beam-induced effects are not so large as the anomalous diffusive effects.

Conclusions

(1) High beta plasma up to β_o = 10% and $\langle\beta\rangle$ = 3% are stably obtained. These values are higher than the critical β values from the ballooning mode analysis.

(2) Up to the power level of 2.2 MW, the increment of β_p is proportional to the net input power. The global energy confinement time τ_E in beam heated plasma appears to be a weak function of plasma density $\bar{n}_e$ and toroidal field B_T. While, the confinement time is significantly improved by increasing plasma current. The

transport in the high beta plasma is nearly the same in a low beta plasma within a factor of 2, i.e. $\chi_e = 3 - 4 \times 10^{17}/n_e$ cm^2/s, $D \approx 0.3\ \chi_e$ and $\chi_i = 3 - 4\ \chi_{NC}$. These experimental results suggest that not only impurity control but also optimization of power deposition profiles of additional heating is very important to improve the global energy confinement time.

(3) Recycling coefficient plays a dominant role in the density clamp.

(4) Plasma rotation does not play an important role in transport processes of high beta plasma in high density region.

(5) Rapid impurity accumulation does not take place during counter-injection. The neoclassical, beam-induced effects are not so large as the anomalous diffusive effects.

ACKNOWLEDGEMENTS

The authors are grateful to Drs. H. Shirakata and S. Matsuda and their crew for developing reliable injectors in a very short period of time and to K. Anno, Y. Matsuzaki and other members of the JFT-2 and the NBI operational groups for their excellent work. They also appreciate stimulating discussions with Drs. N. Fujisawa, Y. Shimomura, A. Funahashi and H. Maeda and are grateful to Drs. S. Mori, Y. Iso, Y. Obata, M. Tanaka, and Y. Tanaka for continuous encouragement.

References

[1] MURAKAMI, M., et al., in Plasma Physics and Controlled Nuclear Fusion Research (Proc. 8th Int. Conf. Brussels, 1980) Vol.1, IAEA, Vienna (1981) 377. Swain, D.W., et al., Nucl. Fusion 21 (1981) 1409.

[2] LEONOV, V.M., et al., in Plasma Physics and Controlled Nuclear Fusion Research (Proc. 8th Int. Conf. Brussels, 1980) Vol.1, IAEA, Vienna (1981) 393.

[3] SUZUKI, N., et al., ibid., 525.

[4] YAMAMOTO, S., et al., Nucl. Fusion 21 (1981) 993.

[5] AZUMI, M., et al., in plasma Physics and Controlled Nuclear Fusion Research (Proc. 8th Int. Conf. Brussels, 1980) Vol.1, IAEA, Vienna (1981) 293.

[6] The JFT-2 Group 10th European Conf. on Controlled Fusion and Plasma Physics, Moscow, 2 (1981).

[7] DIVA Group, Nucl. Fusion 19 (1980) 1219.

[8] MATSUMOTO, H., et al., Nucl. Fusion 22 (1982) 840

[9] SUGIE, T., et al., to be published.

[10] SHIMOMURA, Y., et al., JAERI-M 9065 (1980).

[11] KASAI, S., et al., to be published.

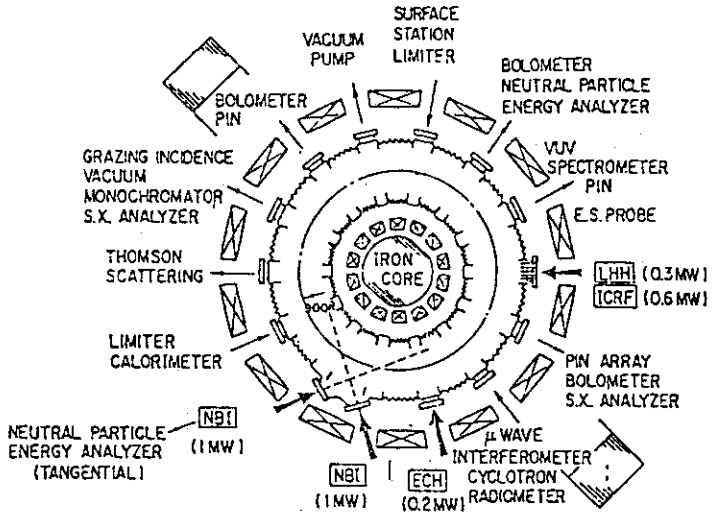

IV-1-1 Additional heating (NBI, ICRF, ECH and LHH) and diagnostic systems in JFT-2 tokamak.

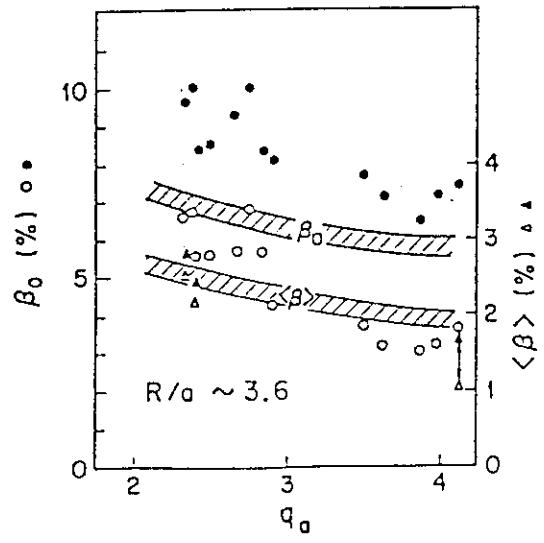

IV-1-2 Critical β values obtained from the ballooning analysis and observed β values. R/a: espect ratio, q_a: safety factor, β_0: peak β and <β>: average β. oΔ: due to thermal component and • ▲: including the beam component in experiment with power of 0.8 - 1.2 MW. ——— : critical peak β value from the analysis and ////// : critical average β value. The lower lines indicate the critical values for q_o = 1 and the upper lines for q_o = 0.9.

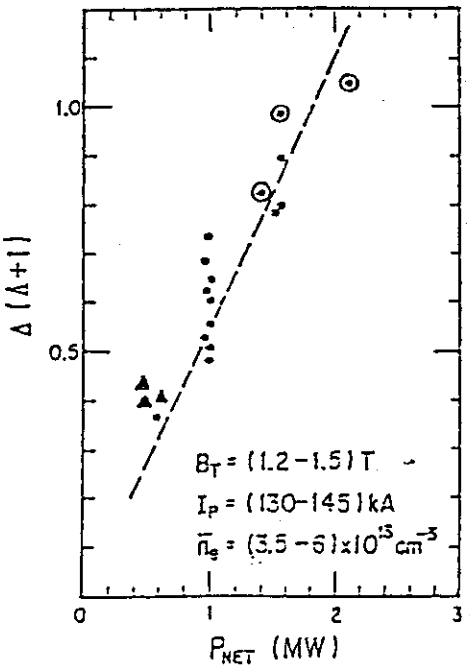

IV-1-3 $\Delta(\Lambda+1)$. v.s. net input power. $\Delta(\Lambda+1)$ is obtained with 4 magnetic probes: NBI + ICRF (●); NBI (○); ICRP (▲)

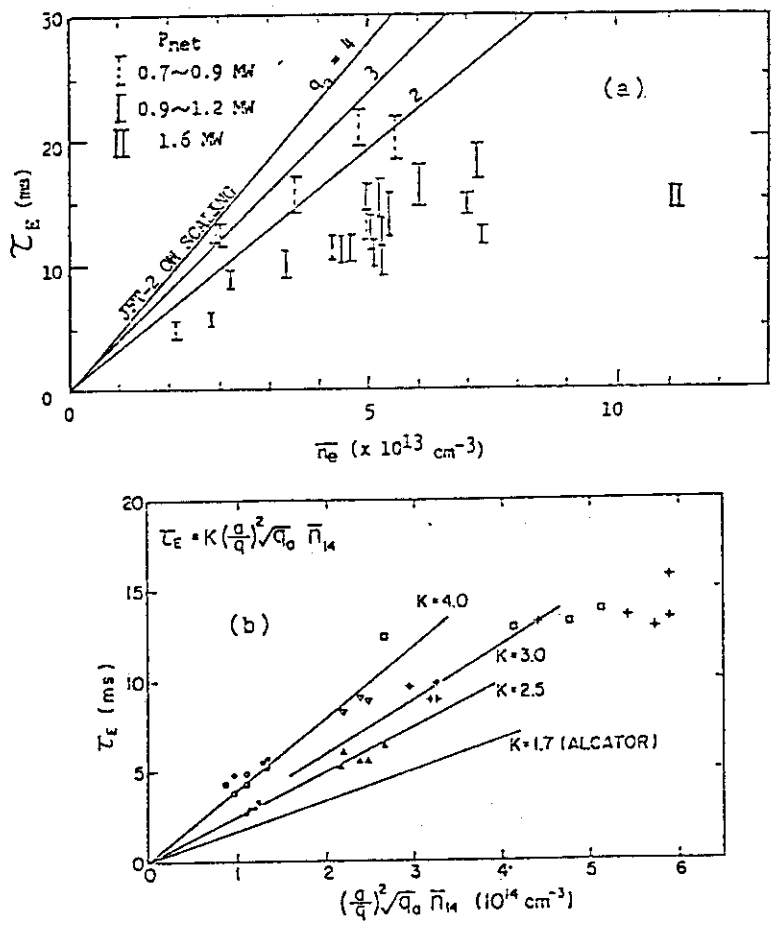

IV-1-4 Global energy confinement time τ_E v.s. plasma density: (a) beam heated discharge, (b) ohmically heat discharge.

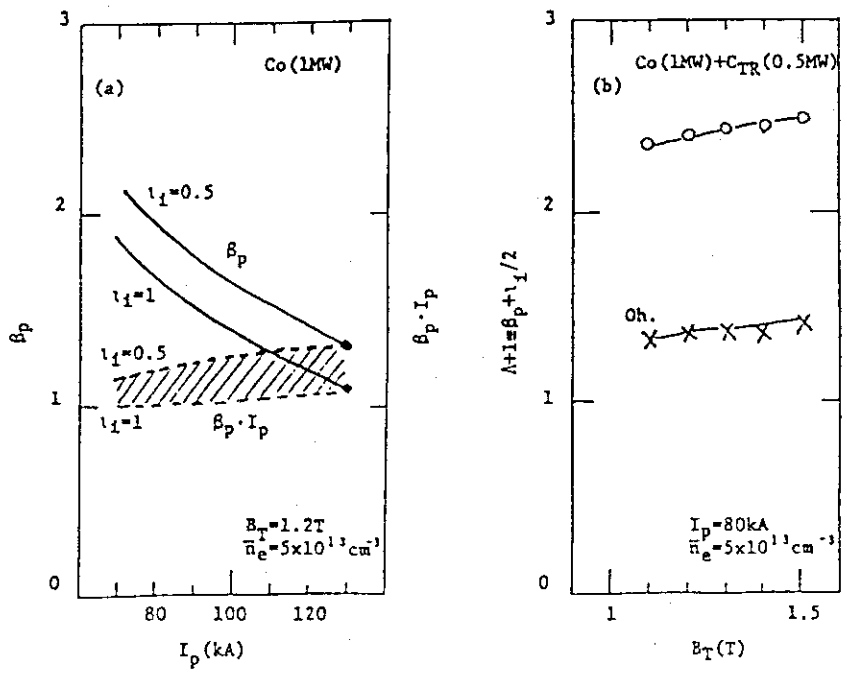

IV-1-5 Fig. 5 (a) Poloidal beta, β_p v.s. plasma current, I_p.
(b) $\Lambda+1$ v.s. toroidal magnetic field, B_T.

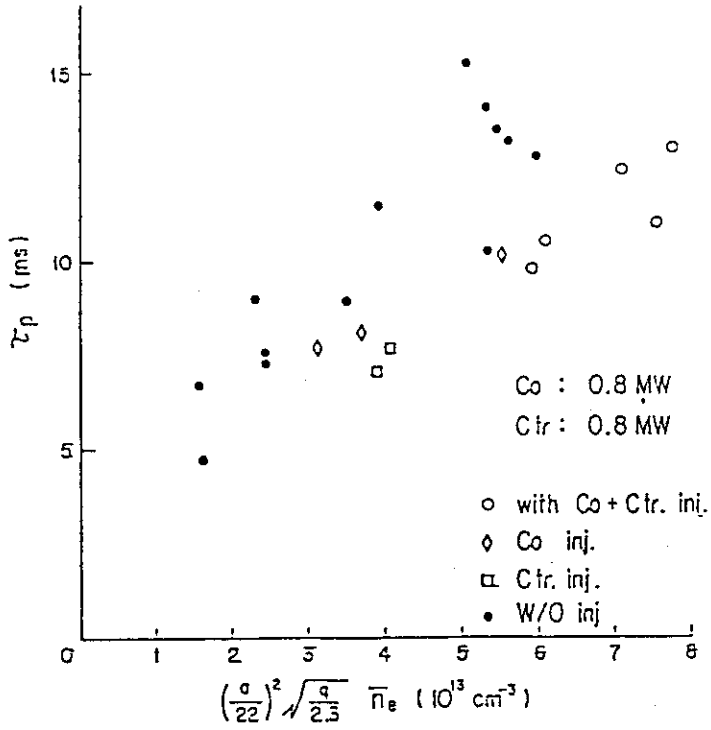

IV-1-6 Global particle confinement time v.s. normalized density, $\sqrt{q}\ \bar{n}_e$.

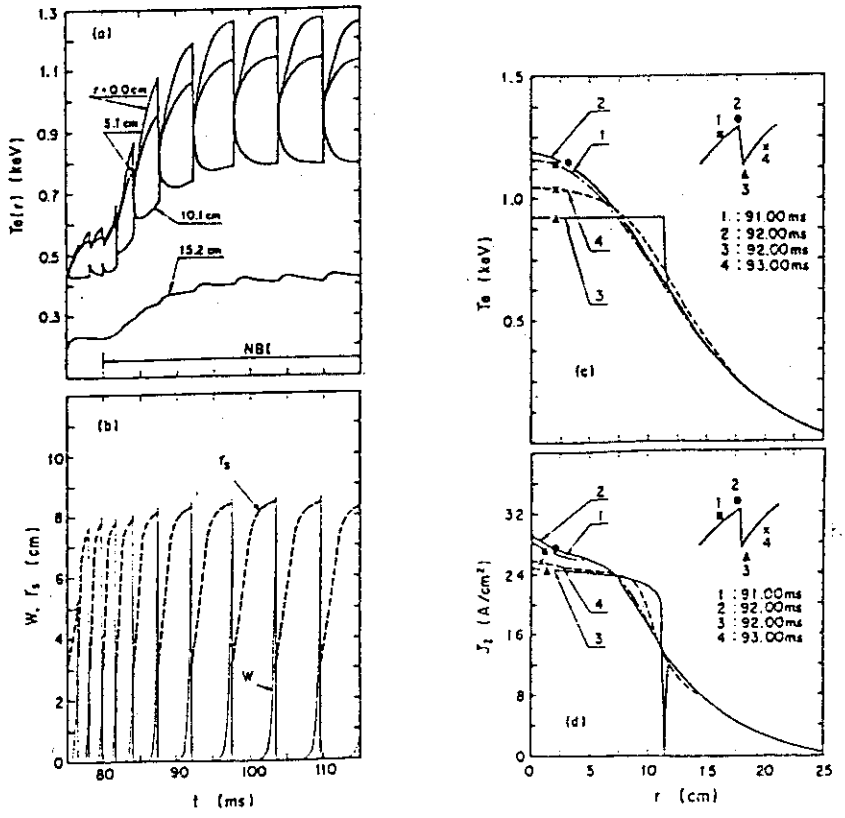

IV-1-7 Example of simulations for beem-induced (enhanced) sawtooth oscillations. Time evolutions of (a) temperature at four raidal position; (b) the position of singular surface, r_s, and island width, W; (c) temperature profiles during sewtooth disruptions; (d) current density profiles during sawtooth disruptions. In this case, diffusion coefficients χ_e, D and χ_i in beam heated discharge is the same as those in ohmically heated discharge.

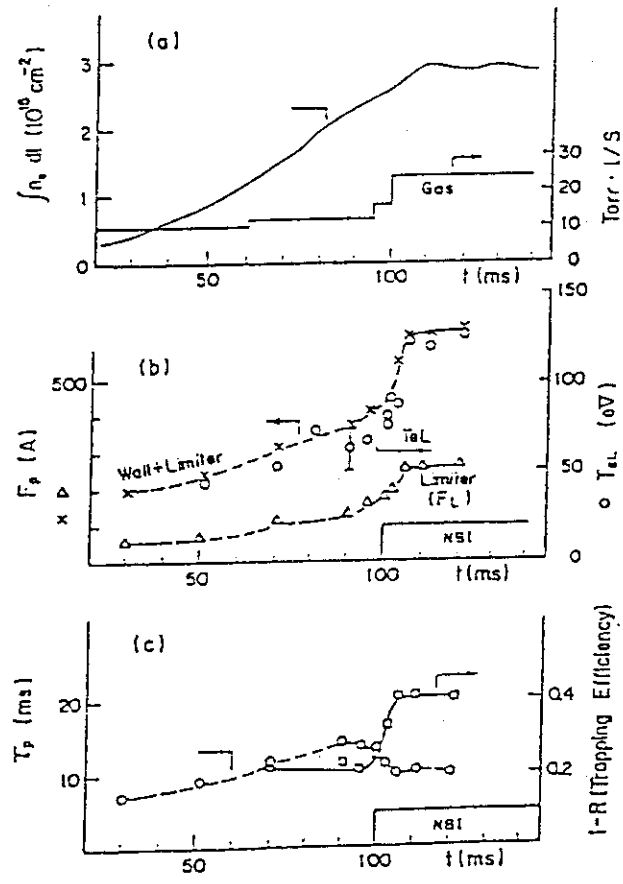

IV-1-8 Density clamping. Time behaviours of particle loss flux, particle confinement time and trapping coefficient. NBI starts from 100 msec. (a) Electron line average density and gas puffing rate. (b) Particle loss flux (Δ; limiter, χ; wall and limiter) and boundary electron temperature (T_{eL}) measured by a electrically biased limiter. (c) Particle confinement time (τ_p) and trapping coefficient (1-R).

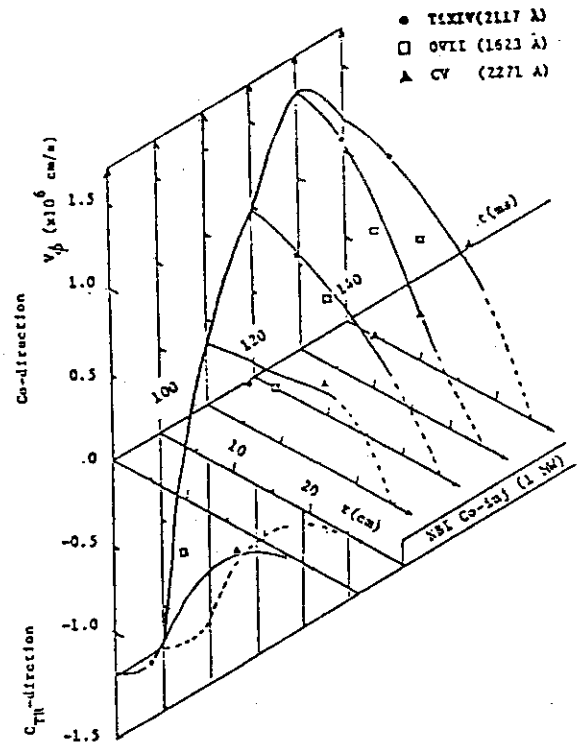

IV-1-9 Measured radial profiles and time evolutions of toroidal plasma velocities. $\bar{n}_e = (3-4)\times 10^{13}$ cm^{-3}, $H^0 \rightarrow E^+$.

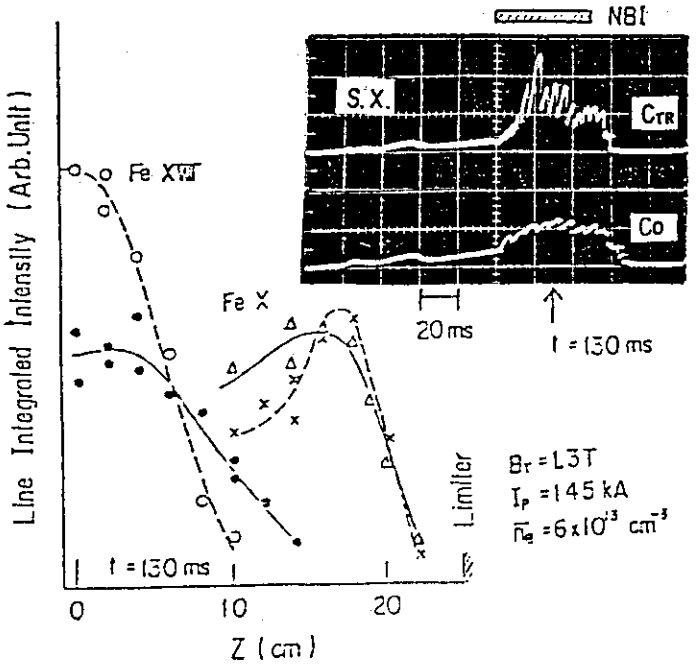

IV-1-10 Line integrated intensity profiles of FeX(174.5 Å) and FeXVIII, (93.9 Å) with co-injection (———) and with counter-injection (-----). Soft x-ray signals along the central chord are also shown.

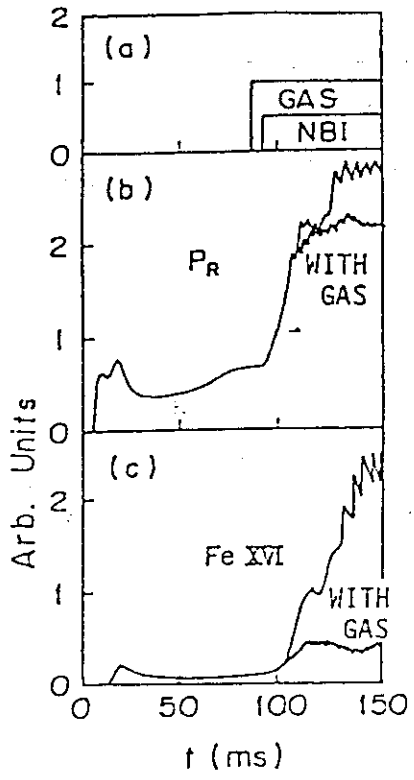

IV-1-11 High-z impurity influx during NBI heating. The NBI heating induces a large influx because of enhanced ion sputtering due to a higher edge temperature. The in fulx is strongly reduced by cooling the edge plasma with an intense gas puffing.

1.1.2 High-β injection experiments with shaped plasmas in Doublet-III

Masayuki NAGAMI

High-β and energy confinement characteristics in beam heated (maximum 2.8 MW) plasmas are compared for D-shaped and circular cross sections. $<\beta_T>$ values in excess of 3% have been obtained with no indication of saturation against beam power in low-q_ψ elongated discharges. With high power heating, the energy confinement time is proportional to I_p, independent of B_T and has a weak dependence on $\bar{n}_e$. It appears that the magnitude of the plasma current is the most essential device parameter determining the energy confinement of beam heated plasmas. For the same B_T, $q_{a\psi}$ and heating power, τ_E and $<\beta>$ increase with elongation, largely due to the increased plasma current allowed in D-shaped plasmas (see reference [A1]).

1.2 Ideal MHD β limit

Takashi TUDA

Stability of Tokamak for high-n ballooning mode is studied.

Combination of a 2-D transport code and an infinite-n ballooning code is used to optimize the beta value (the ratio of the plasma pressure to the magnetic pressure). We get the functional dependence of the maximum beta as

$$\beta(\%) \simeq 7.8\, q_s^{-0.54}\, (A-1)^{-0.76} \varepsilon^{1+0.14(q_s-1)} ,$$

here q_s is the safety factor at the plasma surface, A the inverse aspect ratio, ε the ellipticity of the plasma cross-section (see reference [A2]).

1.3 Conclusions

Data basis of plasma confinement and β limit has been improved by recent neutral beam heating experiments in Doublet III and JFT-II. Doublet III with elongation and aspect ratio similar to the INTOR reference operating point has achieved $<\beta> = 3.3\%$ with no evidence that limiting value is being approached. In Doublet III and JFT-II experiments, the global energy confinement time in beam heated plasma appears to be a weak function of plasma density and toroidal field, while the confinement time is improved by increasing plasma current. Despite the inadequacy of INTOR scaling to describe those parameter dependences, the numerical values of the measured confinement time in the case of similar heating power density to the INTOR case still fit the data relatively well. Thus the INTOR operating plasma parameters need not be changed at this time.

2. Modeling of plasma energetics

2.1 Ripple enhanced ion thermal conductivity

K. Tani

As a part of benchmark calculation, ion thermal conductivity in a a rippled toroidal field is investigated by means of a oribit-following Monte-Carlo code.

2.1.1 Calculation model and assumptions

To evaluate the ion thermal conductivity, plasma is assumed to be circular in cross section and all the magnetic surfaces are concentric circles. Plasma density and temperatures are given to be uniform in space. Ion trajectories are followed by numerical integration of the guiding-center equations. For the convenience of calculations, the effects of high β, electric field, or ripple induced islands on ion orbits are not taken into consideration.

In a Tokamak with finite number of toroidal field coils, the model B field can be described by

$$\vec{B} = B_r(r,\theta,\phi)\vec{e}_r + B_\theta(r,\theta)\vec{e}_\theta + B_\phi(r,\theta,\phi)\vec{e}_\phi \qquad (1)$$

where, r, θ are polar coordinates in the minor cross section of the torus, ϕ is the toroidal anglar coordinate along the magnetic axis and $\vec{e}_r$, $\vec{e}_\theta$, $\vec{e}_\phi$ are the respective unit vectors. The toroidal, poloidal and radial components of the magnetic field are given by

$$B_\phi = B_t \frac{R_0}{R} (1 + \delta(r,\theta)\cos N\phi) \ , \qquad (2)$$

$$B_\phi = \frac{R_0}{R} B_p \ (r), \qquad (3)$$

and

$$B_r = -\frac{1}{rR}\int_0^r \frac{\partial}{\partial\phi}(r'B_\phi)dr' \quad , \tag{4}$$

respectively, where R_0 is the major radius of the magnetic axis, $R = R_0 + r\cos\theta$, B_t the toroidal field on the magnetic axis, B_p the poloidal field produced by plasma current, δ the field ripple and N the number of toroidal field coils.

Since magnetic surfaces are assumed to be concentric circles, the ion thermal conductivity χ_i can be defined as a time differential coefficient of the minor radius variance in the orbit-following Monte-Carlo code, that is,

$$\chi_i = \frac{\Sigma\,(r_i - \langle r_i\rangle)^2\, w_i}{\Delta t\ \Sigma\, w_i} \quad , \tag{5}$$

where

$$\langle r_i\rangle = \frac{\Sigma\, r_i w_i}{\Sigma\, w_i} \quad ,$$

w_i is the energy density weight of the i^{th} test particle and Δt is the calculation time interval.

2.1.2. Calculation results

The ion thermal conductivity defined by eq.(5) describes the total conductivity χ_i^T. The ripple enhanced ion thermal coductivity χ_i^R is assumed to be separated from χ_i^T by

$$\chi_i^R = \chi_i^T - \chi_i^{NC} \quad ,$$

where χ_i^{NC} is the ordinary neoclassical conductivity which is also calculated with the same Monte-Carlo code by switching-off the ripple terms in the guiding-center equations.

About 5,000 test particles are set on a magnetic surface at r/a=0.5 with pitch angle and energy distributions corresponding to an isotropic Maxwellian.

Calculations have been made for the parameters appropriate to INTOR which are summerized in Table IV-2-1. The ion temperature dependence of χ_i^R derived by the Monte-Carlo code is shown in Fig. IV-2-1 by the solid curve. For comparison, theoretical ripple-trapped ion thermal conductivity [1] is also shown by the dotted line in the same figure. The numerical χ_i^R agrees well with the theoretical χ_i^{RT} in the high collisionality regime [2] (low temperature). However, the numerical χ_i^R gradually falls out of the theoretical lines as T_i becomes high and takes a value much smaller than the theoretical χ_i^{RT}.

Table IV-2-1 Plasma parameters

major radius	$R_0 = 5.3$ m
minor radius	$a = 1.2$ m
toroidal field	$B_t = 5.5$ T
plasma temperature	$T_e(r) = T_i(r) = 5.0 \sim 20.0$ keV
	$(T_D(r) = T_T(r) = T_i(r))$
plasma density	$n_e(r) = 1.4 \times 10^{20}$ m^{-3}
	$(n_e(r) = n_T(r) = n_i(r))$
plasma current	$j_p(r) = j_0(1 - (r/a)^2)^2$
safety factor	$q_a = 2.77$
test particles	D^+
ripple	$\delta = \delta_0(r/a)^2 \exp(-0.5\theta^2)$, $\delta_0 = 2\%$
number of toroidal field coils	$N = 12$

2.2 Suprathermal ripple losses

2.2.1 Ripple loss of fast ions produced by NBI

K. Tani

Ripple loss of fast ions produced by NBI during the final phase of beam heating is evaluated numerically by means of orbit-following Monte-Carlo code. Two sets of calculations have been made:

1) Calculations as a part of benchmark tests, in which a model ripple field is used.
2) Calculations in a self-consistent and realistic ripple field which is divergence-free as well as curl-free.

For the convenience of calculations, plasma is assumed to be circular in cross section and all the magnetic surfaces are concentric circles. Ion trajectories are followed by numerical integration of the standard guiding-center equations of motion.

In our orbit-following Monte-Carlo code, Coulomb collisions of fast ions, Coulomb drag and pitch angle scattering on bulk ions and electrons, as well as charge exchange processes with neutral particles are described by means of Monte-Carlo techniques [3]. Since the loss of fast ions due to the field ripple occurs in the very early stage of slowing-down ($\lesssim 0.3\ \tau_s$), it can be separated from the charge exchange loss which is the dominant loss process for slowed-down ions. For this reason, the charge exchange reactions are "switched-off" in the present investigations. Effects of high β, electric field, or ripple induced islands on ion orbits are not taken into consideration.

§1. Loss of fast ions in a model ripple field

The magnetic field used in the present investigations is the same as the one given in the paper entitled "Ripple Enhanced Ion Thermal Conductivity" (see Subsection 2.1). It must be noted that the magnetic filed is divergence-free but still noncurl-free.

Plasma parameters and neutral beam conditions used in the calculations are summarized in Table IV-2-2 and IV-2-3, respectively.

Results are shown in Fig. IV-2-2 for three cases. As the maximum ripple size δ_0 is considerably large and the injection angle is very near perpendicular, very serious losses are predicted.

§2. Loss of fast ions in a realistic ripple field

From the economical point of view, the toroidal field coil system which is small in size and consists of small number of coils has an advantage. In such a system the toroidal field ripple is formed not only in outside but also inside the torus, which is much different from the model field used in the above calculations.

In the present investigation, we employ the same magnetic field that is described in the paper entitled "RIPPLE LOSS OF SUPRATHERMAL ALPHA PARTICLES IN THEIR RELAXATION PROCESS" (see subsection 2.2.2).

Calculations have been made for the case which gives the most serious fast ion loss, i.e., the case (c) in Table IV-2-2. The energy of the major beam particles is 175 keV, other parameters without notice are as those in Table IV-2-2 and IV-2-3. The contour map of fast ion loss derived numerically under the conditions mentioned above is shown in Fig. IV-2-3 in the space of injection angle θ_{inj} and maximum ripple size δ_0 in a plasma (peak-to-average). In a high density plasma with flat distribution, the effective beam heating in the final phase seems

to be very difficult. In order to control the beam power loss fraction below 20%, the maximum ripple size δ_0 should be less than 0.7% and the injection angle θ_{inj} should be greater than 20°. The power loss fraction at $\theta_{inj} = 16°$ and $\delta_0 = 1.2\%$ is about 48%. By comparing the loss fraction with that in Fig. IV-2-2, it can be seen that the ripple formed inisde the torus seems to be unimportant.

Table IV-2-2 Plasma parameters

major radius	$R_0 = 5.3$ m
minor radius	$a = 1.2$ m
toroidal field	$B_t = 5.5$ T
plasma temperature	$T_e(r) = T_i(r) = 15.0(1-(r/a)^2) + 0.1$ keV
	$(T_D(r) = T_i(r) = T_i(r))$
plasma density	$n_e(r) = n_e(0)\ (1-(r/a)^m) + 1.0 \times 10^{19}$ m^{-3}
	$(n_D(r) = n_T(r) = n_i(r))$
	CASE (A): $n_e(0) = 2.1 \times 10^{20}$ m^{-3}, m = 2
	CASE (B): $n_e(0) = 1.3 \times 10^{20}$ m^{-3}, m = 6
	CASE (C): $n_e(0) = 1.8 \times 10^{20}$ m^{-3}, m = 6
plasma current	$j_p(r) = j_0(1-(r/a)^2)^2$
safety factor	$q_a = 2.04$
effective Z	$Z_{eff} = 1.0$
ripple	$\delta = 0.012\ (r/a)^2 \exp(-0.5\theta^2)$
number of toroidal field coils	N = 12

Table IV-2-3 Neutral beam conditions

injection angle	$\theta_{inj} = 16°$ (co-injection)
beam energy	120, 150, 175 keV
species	$P_1 : P_{1/2} : P_{1/3} = 90 : 5 : 5$

2.2.2 Ripple loss of suprathermal alpha particles

The slowing-down process of alpha particles in a rippled toroidal field is investigated by means of an orbit-following Monte-Carlo code. The ripple enhanced power loss fraction of alphas in a reactor-grade tokamak with ∿1% toroidal field ripple may amount to ∿10%. The fraction of particle loss is 1.5 ∿ 1.8 times as large as that of power loss. Almost all the loss alphas escape from a plasma through ripple-enhanced banana drift and ripple-trapped loss particles are negligibly small (see reference [A3]).

The power deposition on the first wall due to ripple loss alphas is roughly estimated at 50 ∿ 70 W/cm^2 for the maximum ripple size δ_0 = 0.75% and ∿150 W/cm^2 for δ_0 = 1.5% (see reference [A4]).

2.3 Neutral beam injection heating power and energy needed to achieve ignition in INTOR

Neutral beam injection heating powers needed to achieve ignition in INTOR are reexamined for the injection energy of 120 keV, 150 keV and 175 keV by one-dimensional transport code. The main purpose of this reexamination is to investigate the possibility to lower the injection energy from the presently specified value of 175 keV.

Model of calculations

We employ the circular plasma, of which minor radius is 1.2 m, to simulate the penetration of the injected beam particles correctly. Instead, the transport coefficients χ are modified to take account of the noncircular effects as

$$\chi \longrightarrow \chi \frac{1}{\kappa} \sqrt{\frac{1+\kappa^2}{2}} \quad ,$$

where κ is the ellipticity. The heating power density is also adjusted to the noncircular plasma. The scrape-off layer plasma is not included and the effect of impurities is ignored for simplicity. The ionized or charge-exchanged fast ions deliver their energy to the field particles instantaneously. The orbit loss of the fast ions and the effect of toroidal field ripple are ignored.

The injection scenario is as follows.

1) Injection anlge ; 16°
2) Beam energy component ; $P_1 : P_{1/2} : P_{1/3} = 90 : 5 : 5$
3) Initial plasma parameters ; $\langle n_O \rangle \sim \langle n_T \rangle \sim 3 \times 10^{19}$ m^{-3}, $I_P = 5.4$ MA

4) Injection time ; 6 seconds

5) Current ramp-up ; $\dot{I}_p \sim 0.16$ MA/s

6) Density ramp-up ; $\langle \dot{n}_e \rangle \sim 1.5 \times 10^{19}$ m^{-3}/s with appropriate pumping

7) Tritium supply ; gas puffing with the energy of 5 eV.

Results of calculations

Ignition approach by NBI heating with the energy of 175 keV, 150 keV and 120 keV are shown in Fig. IV-2-4 ∿ 6 for various injection powers. NBI is started at 7 second. Each dot denotes every 0.5 second. Reference ignition curves for various profiles of ion density and ion temperature are also shown in the figures. These profiles are given by

$$n_i = C_n \bar{n}_i [1 - (r/a)^{\ell_n}]^{m_n}$$

$$T_i = C_t \bar{T}_i [1 - (r/a)^{\ell_t}]^{m_t}$$

From these calculations, it will be concluded that about 75 MW with the energy of 175 ∿ 150 keV should be needed to achieve ignition. Especially, for the case of 120 keV injection energy, about 100 MW injection power will be needed, since, in this calculation, we have ignored various deteriorating effects (scrape-off plasma, ripple loss, impurity effect and so on). It should be investigated further whether these deteriorating effects can be compensated by Shafranov shift.

References

[1] CONNOR, J.W., HASTIE, R.J., Nucl. Fusion 13 (1973) 221.

[2] TANI, I., KISHIMOTO, H., TAMURA, S., in Plasma Physics and Controlled Nuclear Fusion Research (Proc. 8th Int. Conf. Brussels, 1980) vol.1, IAEA, Vienna (1981) 631.

[3] TANI, K., AZUMI, M., KISHIMOTO, H., TAMURA, S., J. Phys. Soc. Japan 50 (1981) 1726.

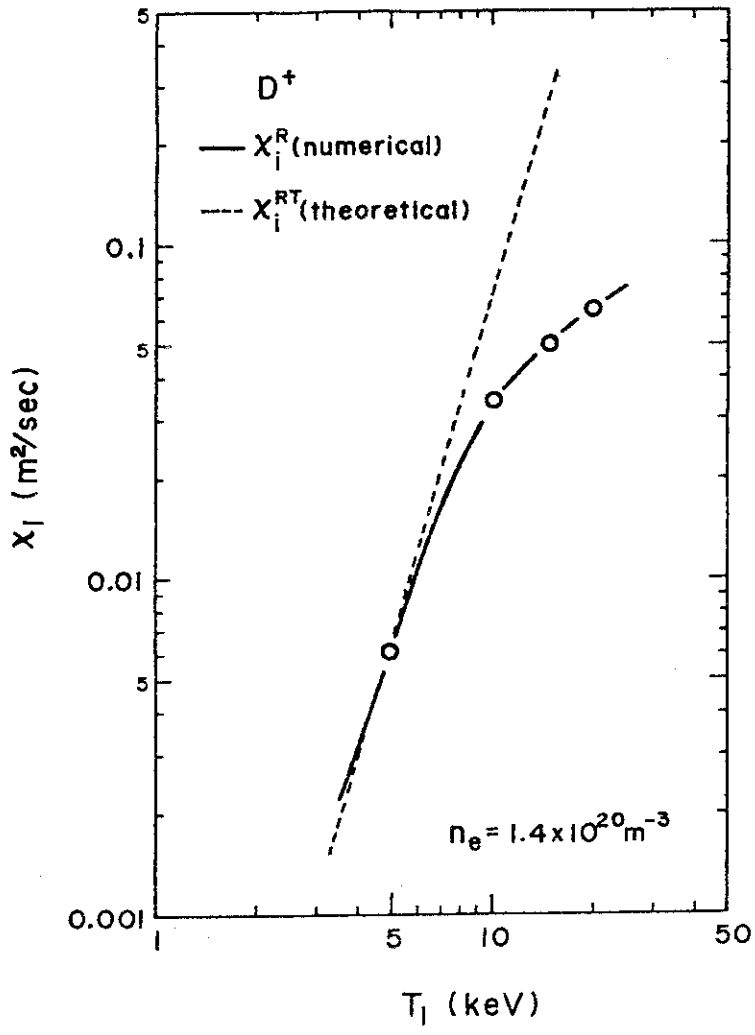

Fig. IV-2-1 Ion thermal conductivity of deuterons as a function of ion temperature at r/a = 0.5. Calculation parameters as in Table VI-2-1.

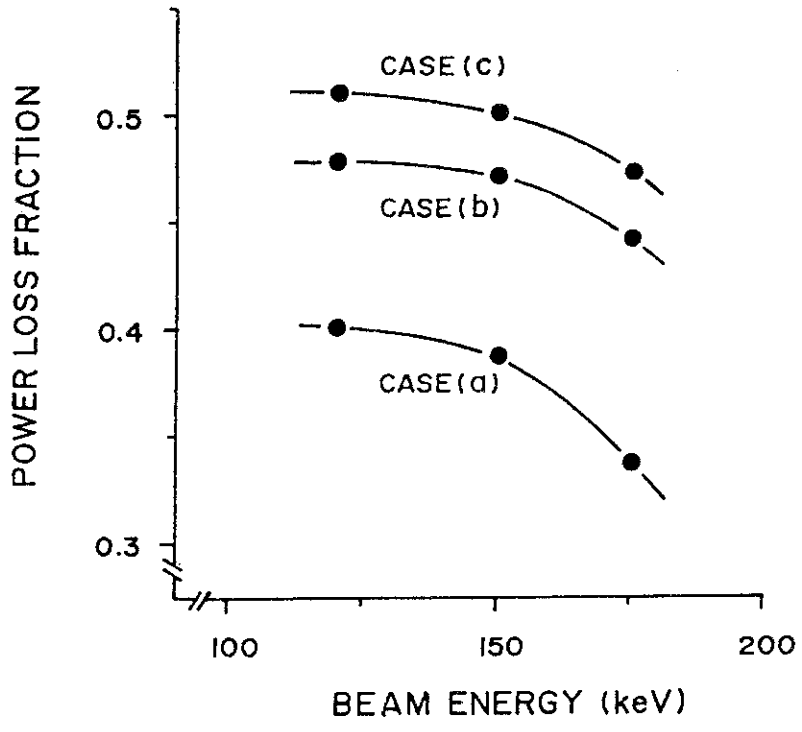

Fig. IV-2-2 Power loss fraction of fast ions produced by NBI against the major beam energy for various plasma density profile:

CASE (A) $n_e(r) = 2.1\times10^{20}(1-(r/a)^2)+ 1.0\times10^{19}m^{-3}$,

CASE (B) $n_e(r) = 1.3\times10^{20}(1-(r/a)^6)+ 1.0\times10^{19}m^{-3}$,

CASE (C) $n_e(r) = 1.8\times10^{20}(1-(r/a)^6)+ 1.0\times10^{19}m^{-3}$.

Other parameters as in Table VI-2-2~3.

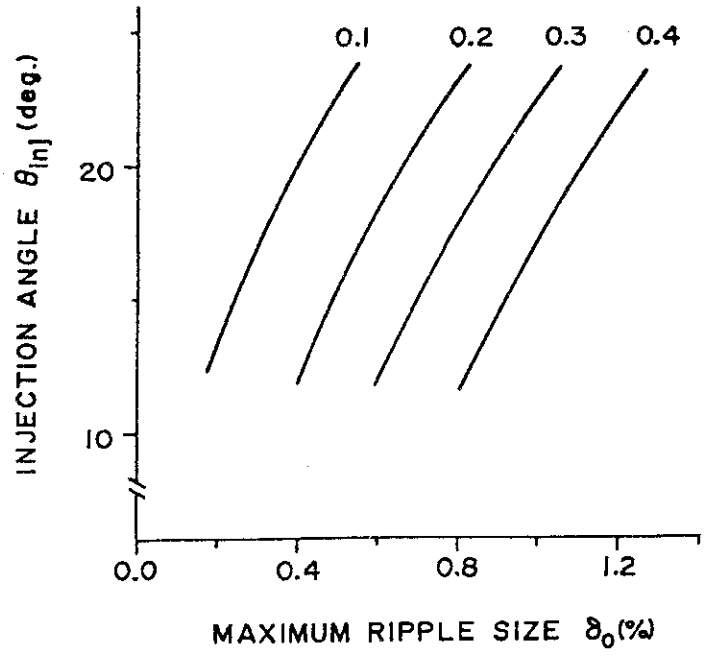

Fig. IV-2-3 Contour map of power loss of fast ions in the space of maximum ripple size δ_0 and injection angle with respect to perpendicular θ_{inj}. The plasma density profile is given by $n_e(r) = 1.8\times10^{20}(1-(r/a)^6)+1.0\times10^{19}m^{-3}$ (CASE (C)), and the major beam energy is 175 keV.

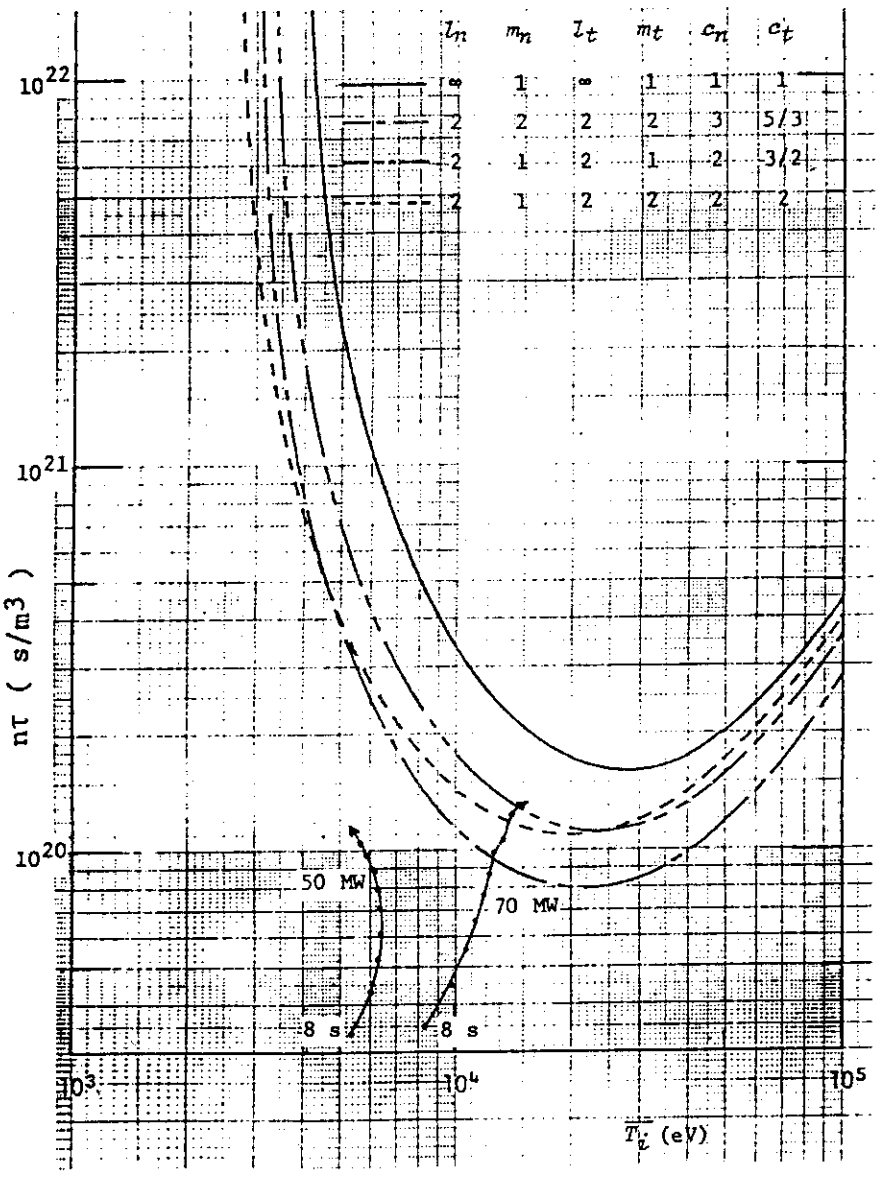

Fig. IV-2-4 Ignition approach by NBI heating of 175 keV injection energy. Injection power of about 70 MW will be required to ignite the plasma. NBI is started at 7 seconds. Each dot denotes every 0.5 seconds.

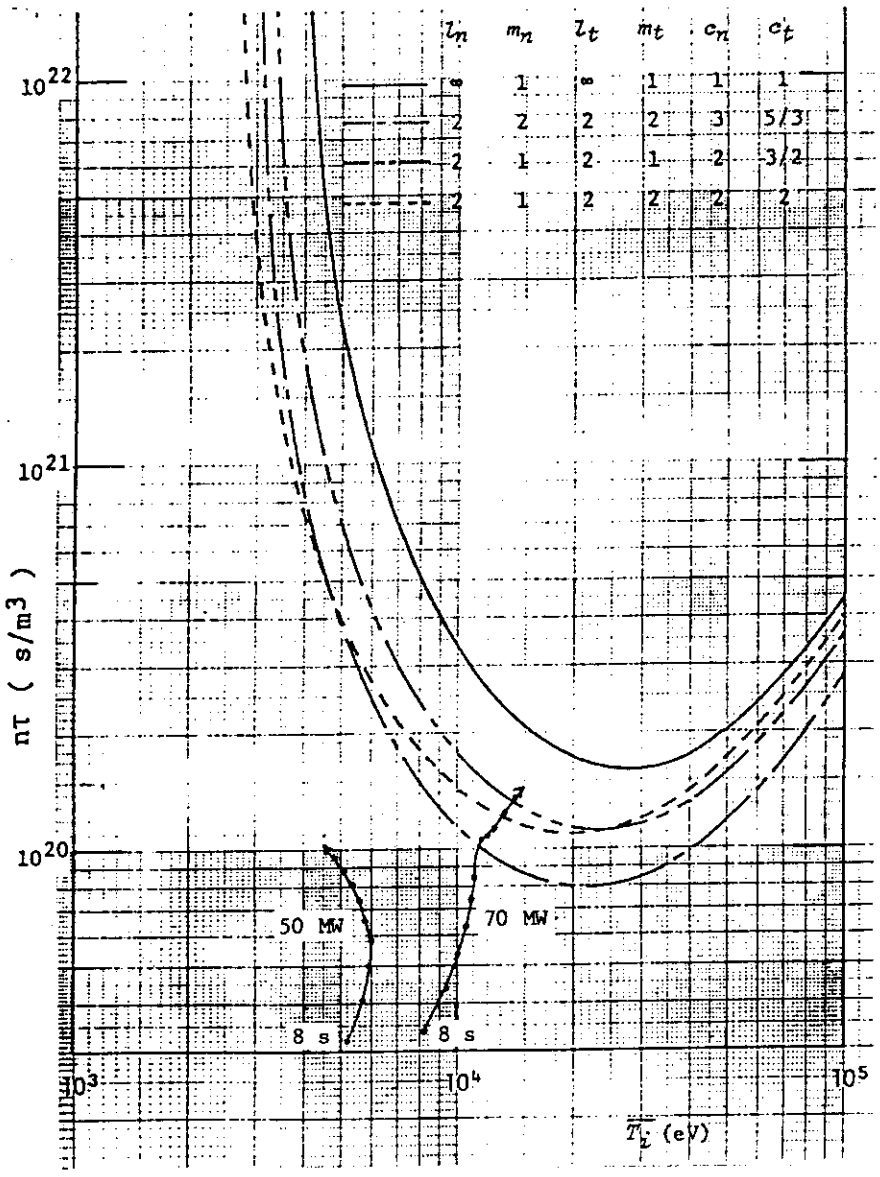

Fig. IV-2-5 Ignition approach by NBI heating of 150 keV injection energy. Injection power of about 70 MW will be required to ignite the plasma. NBI is started at 7 seconds. Each 0.5 seconds.

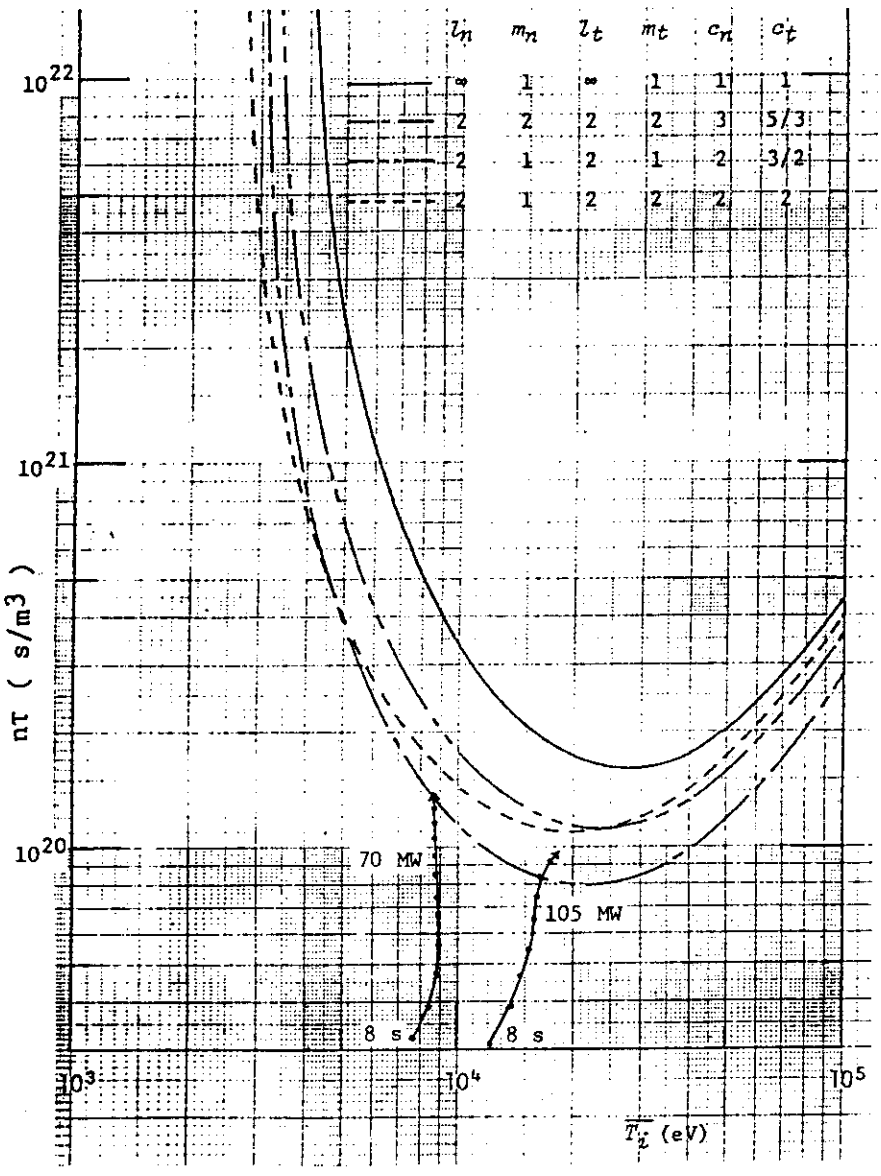

Fig. IV-2-6 Ignition approach by NBI heating of 120 keV injection energy. Injection power of about 100 MW will be required to ignite the plasma successfully since various deterioration effects must be considered. NBI is started at 7 seconds. Each dot denotes every 0.5 seconds.

3. Discharge Control Issues

3.1 Burn temperature control with compression-decompression

Masao OKAMOTO

The active feedback control by means of major radius compression-decompression has been studied for the purpose of burn control in a self-ignited tokamak. Based on a zero-dimensional transport equations, together with a simple but realistic feedback control system which regulates the vertical magnetic field applying compression-decompression to the plasma, numerical calculations have been carried out for Alcator, Coppi-Mazzucatto and Hirshman-Molvig scalings taking an INTOR-like tokamak as an example. It is shown that the feedback control can move the plasma automatically to the marginal ignition point from the sub- or supper-ignited region after the additional heating is stopped. Once the plasma has bound the marginal ignition point, the control can maintain its operation point suppressing the thermal instability completely without changing the major radius. Linear stability analysis for general type of scalings has shown that the control is achievable for suitable gain even if the time lag of the system is longer than the thermal runaway time. Dependences of the stability on scaling laws are also stuided. It is demonstrated from a numerical example that varying the fusion output power level during the operation is possible without bringing about the thermal runaway (see reference [A5]).

3.2 Equilibrium control requirement

Kojyu UEDA

Both of the shell effect due to passive shell-structures and the characteristic of simplified feedback control systems, for the vertical position stabilization of the elongated INTOR plasma, are studied and the following matters have been obtained.

Inductive components with the systems consist of shells, shields and control coils. Both of the shells and shields are toroidally divided into 24 sectors.

A new type of retangular shell, which has the sufficient shell effect for the stabilization of the fast mode, is presented here on a basis of the studies of various kinds of shell-structures described on this paper in detail, and used as the shell structure.

It is found that the rectangular shells can be formed so as to effect on the bleeding ratio only by a negligible small by locating them separately on both of the front and rear surfaces of blanket.

Some properties with the modelled feedback control system are studied under a disturbance field, $B_d = B_\infty \cdot [1 - \exp(-t/\tau_d)]$ (B_∞: field strength at $t = \infty$, τ_d: time constant). They are studied for two kinds of decay indices, that is, -1.0 for the pump limiter and -1.3 for the divertor.

Conclusively, the control system is found to have good characteristics. The PID controller seems to provide the stable control of vertical position better than the PI controller.

Due to the method in this paper, the maximum of vertical displacement, Z_p^{max} under the disturbance field, B_d, are in proportion to B_∞.

Also the power requried for its stabilization, P are in proportion to B_∞^2, and then to $(Z_p^{MAX})^2$, too. Therefore, some common basis for B_∞ or Z_p^{MAX} is found to be required for its estimation.

Moreover, P is found to be independent of whether the PI or PID controller is used, and to be on a curve in relation with Z_p^{MAX}. The difference of P between -1.0 and -1.3 in n is very large in Z_p^{MAX} more than -1.0 cm. For example, in the vicinity of $Z_p^{MAX} = 1.0$ cm, P in the case of n = -1.0 is about one half times in the case of n = -1.3. But it seems to decrease abruptly in Z_p^{MAX} less than 0.5 cm (see reference [A6]).

3.3 Disruption characteristics and control

— Demonstration of High Density, Low-q Discharges with D-shaped Plasmas in Doublet II and Their Toughness for Disruptions —

Masayuki NAGAMI

For a takamak reactor, which needs a several percent in a beta value, we intend to increase the beta value by taking advantage of elongating a plasma and reducing a safety factor, which is predicted by theoretical ballooning mode studies. The INTOR conceptual design also expects a high beta plasma $\beta_T = 5 - 6\%$ with the ellipticity $k = 1.6$, the simple safety factor $q_I = 2.0$ without toroidal effect, and the plasma density with its Murakami coefficient $C_N = 14$.

Needless to say, there is no precedent for demonstrating the above plasma parameters at the same time. Such high endsity and low-q discharges, furthermore, might be fragile for disruptions.

The attached paper describes the discharge properties of the D-shaped, high density and Low-q plasmas achieved in Doublet III. The obtained results, which is, however, for Joule heated plasmas, suggest the possibility of realizing the INTOR discharges with high elongation, high density, low-q. The disruption frequency data are also helpful of making a specification of the INTOR operation scenario.

The results of the Doublet III experiments could be summarized as follows,

1) The simple safety factor $q_I = 1.5$ is demonstrated for 1.5 elongated D-shaped plasmas. The actual safety factor (q_ψ) might exceed two, because of strong toroidal effect at the plasma edge.

2) We also demonstrate the high density operational capability of the Murakami's coefficient reaching 7.8 in the low-q, D-shaped plasmas, and their average beta value reaches one percent.

3) The stable discharges with $q_I > 2$ could be reproducible without disruptions with extremely high probability, once we could find the stable operation conditions. Reducing q_I less than 2, the disruption frequency increases, and the discharges with $q_\psi \simeq 2$ can hardly escape the disruptions.

Judging from the above results, the present INTOR plasma parameters, i.e., $q_I = 2.0$, $K = 1.6$, $C_N = 14$, could be realized without suffering disruptions, taking account of the expected improvements achieved in the future large tokamaks (see reference [A7]).

4. Conclusions

As far as plasma confinement and beta limit are concerned, the data base has been improved by recent neutral beam heating experiments in Doublet III and JFT-II. As is described in section 1.3 the global energy confinement times in beam heated plasma appears to be a weak function of plasma density and toroilda field, while the confinement time is improved by increasing plasma current. Despite the inadequency of INTOR scaling to describe these parameter dependences, the numerical values of the measured confinement time in the case of similar heating power density to the INTOR case still fit the data relatively well. Thus the INTOR operating parameters need not be changed at this time.

Toroidal field ripple losses of bulk plasma, fast ions produced by neutral beam injection and alpha particles are evaluated by Monte-Carlo code. When applied to INTOR case, thermal ripple losses are not an important factor in the energy balance at the ripple levels under consideration. The ripple induced fast ion losses for neutral beam heating is estimated to be 40-50 % of the injected power in the case of injected energy 150 keV at toroidal ripple δ = 1.2 % at the plasma edge. Detail analysis of alpha particle losses is performed. The power loss is predominantly in particles of energy in excess of 3 MeV and the losses are localized in the region near outboard midplane in the plane of the toroidal field ocils. The power loss at toroidal ripple δ = 1.2 % at the plasma edge amounts to 15-25 % of the alpha power and reaches values is excess of 1 MW/m^2 corresponding to a peaking factor of around 20. We conclude that δ = 1.2 % design specification appears compatible with physics requirement but the further analysis on a fast-ions and alpha losses is necessary.

Burn temperature control by compression and decompression is analyzed. This method may be one of the candidates of burn temperature control. Further analysis is necessary on such as density control by changing the recycling condition and pellet injection, beta limits or control of ripple induced losses.

The model calculations on the effectiveness of passive loop on vertical position control is performed and it is shown that 24-toroidal

segments of passive loop can be used effectively. The characteristics of feedback system of vertical position control using active coils with the passive loop is analyzed and the feasibility of vertical position control of these system is confirmed.

Acknowledgements

The authors are grateful to the members in Fusion Research and Development Center for their excellent works and stimulating discussions. They are also grateful to Drs. S. Mori, Y. Iso, Y. Obata, and K. Tomabechi for their continuous encouragement.

segments of passive loop can be used effectively. The characteristics of feedback system of vertical position control using active coils with the passive loop is analyzed and the feasibility of vertical position control of these system is confirmed.

Acknowledgements

The authors are grateful to the members in Fusion Research and Development Center for their excellent works and stimulating discussions. They are also grateful to Drs. S. Mori, Y. Iso, Y. Obata, and K. Tomabechi for their continuous encouragement.

References

[A1] M. Nagami and the JAERI TEAM, D. Overskei and the GA TEAM, in Plasma Physics and Controlled Nuclear Fusion Research (9th Conf. Baltimore, 1982) IAEA-CN-41/A-2.

[A2] T. Tuda, M. Azumi, G. Kurita, T. Takizuka, and T. Takeda, JAERI-M 82-104 (1982).

[A3] K. Tani, T. Takizuka, M. Azumi, and H. Kishimoto, "Ripple Loss of Suprathermal Alpha Particles in their Relaxaton Process" to be published somewhere in near future.

[A4] K. Tani, "Ripple Loss of Suprathermal Alpha Particles in their Relaxation Process (II)" to be published in combination with the above reference [A3].

[A5] M. Okamoto, M. Ohnishi, K. Hirano, and T. Amano, in Plasma Physics and Controlled Nuclear Fusion Research (9th Conf. Baltimore, 1982) IAEA-CN-41/0-5.

[A6] K. Ueda, S. Nishio, N. Fujisawa, M. Sugihara, S. Saito, and K. Miyamoto, "Vertical Position Control of the Elongated INTOR Plasma" to be published in JAERI-M.

[A7] M. Nagami, H. Yoshida, K. Shinya, G. Jahns, H. Yokomizo, M. Shimada, K. Ioki, S. Izumi, and A. Kitsunezaki, JAERI-M 9589 (1981).

[N1] Japanese Contributions to IAEA INTOR Workshop, Phase IIA, Chapter I: Introduction, Chapter II: Summary and Recommendation, Chapter III: INTOR Concept, JAERI-M 82-170.

[N3] Japanese Contributions to IAEA INTOR WOrkshop, Phase IIA, Chapter IV: Plasma Confinement and Control, JAERI-M 82-171.

[N3] Japanese Contributions to IAEA INTOR Workshop, Phase IIA, Chapter V: RF Heating and Current Drive, JAERI-M 82-172.

[N4] Japanese Contributions to IAEA INTOR Workshop, Phase IIA, Chapter VI: Impurity Control Physics, JAERI-M 82-173.

[N5] Japanese Contributions to IAEA INTOR Workshop, Phase IIA, Chapter VII: Impurity Control and First-Wall Engineering, JAERI-M 82-174.

[N6] Japanese Contributions to IAEA INTOR Workshop, Phase IIA, Chapter VIII: Tritium and Blanket, JAERI-M 82-175.

[N7] Japanese Contributions to IAEA INTOR Workshop, Phase IIA, Chapter IX: Magnets, JAERI-M 82-176.

[N8] Japanese Contributions to IAEA INTOR Workshop, Phase IIA, Chapter X: Electromagnetics, JAERI-M 82-177.

[N9] Japanese Contributions to IAEA INTOR Workshop, Phase IIA, Chapter XI: Mechanical Configurations, JAERI-M 82-178.

[N10] Japanese Contributions to IAEA INTOR Workshop, Phase IIA, Chapter XII: Engineering Testing, JAERI-M 82-179.